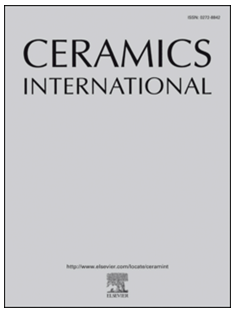

3D printing of Nd: YAG transparent composite ceramics

Haohao Ji, Mengmeng Xie, Yu Liu, Nianjiang Chen, Shiwei Wang, Dianzi Liu, Wenlan Gao, Haoran Wang, Yanhao Dong, Jian Zhang

PII: S0272-8842(25)01582-2

DOI: https://doi.org/10.1016/j.ceramint.2025.03.430

Reference: CERI 46285

To appear in: *Ceramics International*

Received Date: 27 November 2024

Revised Date: 17 March 2025

Accepted Date: 29 March 2025

Please cite this article as: H. Ji, M. Xie, Y. Liu, N. Chen, S. Wang, D. Liu, W. Gao, H. Wang, Y. Dong, J. Zhang, 3D printing of Nd: YAG transparent composite ceramics, *Ceramics International*, https://doi.org/10.1016/j.ceramint.2025.03.430.

3D printing of Nd: YAG transparent composite ceramics

Haohao Ji[a,b], Mengmeng Xie[c], Yu Liu[c,*], Nianjiang Chen[d], Shiwei Wang[a,b], Dianzi Liu[e,*], Wenlan Gao[a], Haoran Wang[a], Yanhao Dong[f], Jian Zhang[a,b,*]

[a]*State Key Laboratory of High Performance Ceramics and Superfine Microstructure, Shanghai Institute of Ceramics, Chinese Academy of Sciences, Shanghai 200050, China*

[b]*Center of Materials Science and Optoelectronics Engineering, University of Chinese Academy of Sciences, Beijing 100049, China*

[c]*School of Mechanical Engineering, Jiangnan University, Wuxi 214122, Jiangsu, China*

[d]*Science and Technology on Solid-State Laser Laboratory, Beijing 100015, China*

[e]*School of Engineering, University of East Anglia, NR4 7TJ, Norwich, UK*

[f]*State Key Laboratory of New Ceramics and Fine Processing, School of Materials Science and Engineering, Tsinghua University, Beijing 100084, China*

[*]Corresponding authors.

E-mail: Y Liu, yuliu@jiangnan.edu.cn;

D Liu, Dianzi.Liu@uea.ac.uk;

J Zhang, jianzhang@mail.sic.ac.cn

Abstract: The application of 3D printed transparent composite ceramics with designable gain profile in solid-state lasers has garnered increasing interest. Problems including the poor performance of slurries, defects generated in the green bodies during printing and the uncontrolled densification process between ceramics with different components have deteriorated the optical quality of transparent composite ceramics prepared by direct ink writing (DIW), leading to the limitations on the realization of high-power laser outputs. To solve this problem, a systematic investigation of Nd: YAG transparent composite ceramics was conducted throughout the fabrication process, including DIW with the capability of dual-material switching, vacuum sintering and hot isostatic pressing (HIP). First, the ceramic slurries with good printability and high solids loading were formulated by adjusting the dispersant and thickener contents. The sintering behaviors of undoped YAG and Nd: YAG ceramics were investigated to enhance the optical quality of transparent composite ceramics. The Nd ions diffusion distances of the interface between undoped YAG and Nd: YAG regions in the vertical and horizontal composite ceramics were tested and calculated to be 50.1 μm and 43.5 μm, respectively. Finally, the laser measurement of the YAG/0.3 at. % Nd: YAG/YAG transparent composite ceramic with the dimension of 3×3×4 mm^3 indicated that the maximum output power of 2.15 W with the slope efficiency of 40.2% was achieved at the absorbed pump power of 5.70 W.

Keywords: Transparent ceramics, YAG, Composites, Direct ink writing

1. Introduction

The solid-state laser has been widely used in high energy density physics, laser fusion, machining and defense applications due to its compact structure, ease of use and high output power [1-3]. As the most important part of solid-state lasers, the gain medium determines the laser performances to a great extent. In comparison of the laser glass or laser crystal, laser ceramic has the advantages including the high maximum dopant concentration and excellent thermomechanical property. In 1995, Ikesue et al. first demonstrated the efficient laser oscillation in use of Nd: YAG transparent ceramics [4], which opened the way for laser ceramics to serve as gain medium for high power solid-state lasers.

Usually, the solid-state laser operates in either a continuous or pulse mode. In this process, a part of the pump power is converted into the laser output, and the rest energy is consumed in the form of heat generation. For the uniformly doped Nd: YAG transparent ceramics, the absorbed pump power density gradually decreases from both ends to the center. In a worse scenario, the unevenly absorbed pump power density in laser gain media can lead to an uneven temperature distribution, which causes mechanical and thermal stresses as well as the variation of refractive index. In Refs. [5-7], the thermal induced birefringence, thermal lens effect and thermal induced depolarization were investigated to evaluate their impacts on the laser output power and beam quality. Recently, assembling transparent ceramics into a composite structure is becoming a promising method to effectively improve the total energy storage density and minimize such thermal effects of the gain media [3]. Specifically, the thermal

conductivity of undoped ceramics is higher than that of doped ceramics, thereby accelerating heat dissipation.

The traditional preparation methods for the fabrication of transparent composite ceramics include dry pressing and tape casting [8-12]. In the dry pressing method, undoped YAG powders, RE: YAG powders and undoped YAG powders are charged into a mold in order and uniaxially pressed. Then, the powder compact is cold isostatically pressed into a ceramic green body. In 2008, Ikesue et al. prepared gradient doped Nd: YAG ceramics by dry pressing and realized a laser output with a slope efficiency of 40% [3]. Results showed that the gradient doping made the pump power density and thermal field distribution of the gain medium more uniform. Li et al. reported the fabrication of a Nd: YAG composite ceramic slab by dry pressing based on the theoretical design of the doping concentration and the doping length [13]. The double-pass extracted power of the ceramic slab in the laser amplifier was higher than 7 kW and the optical to optical conversion efficiency was equivalent to that of the uniformly doped crystal slab. However, the precise interface control between the undoped and doped regions and the repeatability are the major limitations in this method. For tape casting, it is necessary to prepare ceramic slurries with different components. The tapes are cut into pieces that are stacked and laminated into green parts. Messing et al. reported for the first time that a transparent composite ceramic rod consisting of undoped YAG, 0.25 at. % Er: YAG and 0.5 at. % Er: YAG was prepared by tape casting [14]. A quasi-continuous laser output of 7 W at 1645 nm was obtained with the optical to optical conversion efficiency of 56.9%. However, massive organic

agents had to be used for the preparation of high quality tapes.

In recent years, 3D printing technique as an excellent forming method, has been developed to fabricate ceramics with a complicated shape or internal composition distribution [15, 16]. Especially, direct ink writing (DIW) has attracted extensive attention in the field of transparent ceramics, as DIW has the manufacturing flexibility to control the composition distribution in the target structure [17-22]. In 2018, the ceramic gain medium comprised of a central core of Nd: YAG and an undoped cladding region of YAG was fabricated by DIW [21]. Later, Lutetium and Gadolinium were chosen as optically-inert co-doping ions in the fabrication of transparent composite ceramics to match the increase in refractive index caused by Neodymium [17]. It is noted that the dopants in YAG must be carefully managed. Also, the as-deposited doping geometry is affected by ionic diffusion under the high temperatures required to densify the powders into transparent ceramics. Moreover, the combination of DIW with other technologies, such as ultraviolet [23], low-temperature [24], active mixing [25], etc., could generate transparent ceramics with interior design flexibility in structure and composition distribution, enabling new opportunities for the future development and applications. However, the slurries commonly used in DIW have disadvantages, such as containing excessive organics and poor printability, causing defects in the green bodies that cannot be eliminated during sintering [18, 21, 22]. Also, the sintering densification processes of ceramics with different components cannot be effectively controlled [9]. These all lead to the poor optical quality of the transparent composite ceramics fabricated via DIW and the inability to realize effective laser outputs.

In the present work, taking the strategy of cellulose thickening, ceramic slurries with high solids loading and good printability were formulated using only a small amount of organic matter and green bodies without defects were obtained. Also, the sintering densification processes of different components in the composite ceramics were strictly regulated to improve transparency. Finally, both the Nd ions diffusion behaviors across interfaces and the laser output of transparent composite ceramics were assessed to demonstrate the effectiveness and feasibility of the proposed method for the fabrication of advanced transparent composite ceramics.

2. Experimental

2.1. Materials

The ceramic powders were obtained by mixing α-Al_2O_3 (99.99 wt. % purity, Taimei Chemical Co., Ltd., Japan), Y_2O_3 (99.99 wt. % purity, Jiahua Advanced Material Resouces Co., Ltd., Jiangyin, China) and Nd_2O_3 (99.99 wt. % purity, Aladdin Biochemical Technology Co., Ltd., Shanghai, China) powder according to the stoichiometry ratios of $Y_3Al_5O_{12}$ and $Y_{2.991}Nd_{0.009}Al_5O_{12}$, respectively. At the same time, SiO_2 was added in the form of 0.5 wt. % tetraethyl orthosilicate (TEOS, Sigma-Aldrich, 99.999%) as sintering additives. The powders were ball-milled in ethanol for 12 h. The slurry was dried in an oven for 24 h and sieved through an 80-mesh grid. More details have been provided in Ref. [26]. Fig. 1 shows the SEM micrographs and energy dispersive spectra of the mixed powders. It can be observed that the alumina powder, yttrium oxide powder and neodymium oxide powder were uniformly mixed after ball milling. Following that, to obtain two kinds of slurries with low viscosity, the pre-mixed

powders were milled using a planetary ball mill (QM-3SP4, Nanjing Nanda Instrument Co., Ltd., China) with dispersant (Dolapix CE - 64, Zschimmer & Schwarz, Germany), deionized water and alumina balls in a 500 mL nylon jar at the speed of 250 rpm for 1 h. Hydroxyethyl cellulose (HEC, powder, 3400–5000 mPa·s at 25 °C, Shanghai Macklin Biochemical Co., Ltd., China) was added to the ball-milled slurries to improve the printability. The slurries were then mixed uniformly and degassed by a vacuum mixer. Finally, the slurries were loaded into the syringes and degassed by a vacuum mixer to avoid defects in the samples caused by air bubbles.

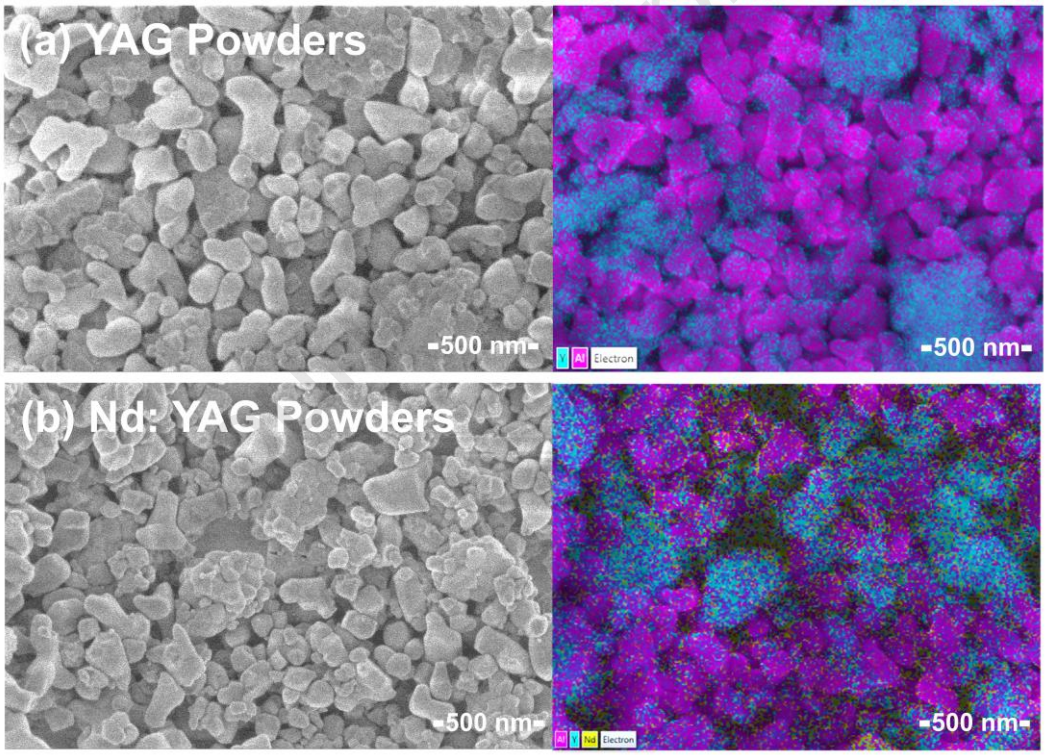

Fig. 1. SEM micrographs and energy dispersive spectra of the mixed (a) YAG and (b) 0.3 at. % Nd: YAG powders.

2.2. Preparation of green bodies and ceramics

In order to prepare transparent composite ceramics, DIW with the capability of dual-material switching was designed and fabricated. The device that was composed of jigs

and a pneumatic sliding table, was integrated with the corresponding control program to realize the DIW using two materials. The experiments were carried out on a homemade DIW printer, which was consisted of a computer-controlled 3-axis gantry platform and a feeding system with two independent electric proportional valves shown in Fig 2(a), and the printing path was defined in Fig. 2(b). The syringes filled with the two slurries were fixed on jigs with the height difference to avoid the mutual interference between nozzles and samples during printing. First, the undoped YAG slurry was used to print and then the jig was vertically lifted up under the control of the program. Then, the syringe filled with the Nd: YAG slurry was moved downward using the pneumatic sliding table to stagger the two syringes in the vertical direction so that the scratching between nozzles and samples could be prevented during printing. Following that, the needle filled by the Nd: YAG slurry was positioned by the three-dimensional coordinates where the needle filled by the undoped YAG slurry was located under the control of the program. Thus, the Nd: YAG slurry was printed. It should be noted that the 3D coordinates of the two nozzles must be corrected every time before printing. Finally, the jig was lifted vertically, and the pneumatic sliding table was reset. The printing process of transparent composite ceramics can be demonstrated in Fig. 2(c). The slurries were deposited on a glass plate coated with Teflon. To control the drying process, the printed wet ceramic green bodies were covered with polyethylene lids and then placed in a chamber at the temperature of 25 °C and the relative humidity of 85% for 48 h.

The dried green bodies were heat treated at 800 °C for 6 h to remove the organic

additives and then pre-sintered at different temperatures for 6 h under vacuum of 10^{-3} Pa in the furnace equipped with a tungsten mesh as the heating element. In order to eliminate the residual pores completely, the samples were further hot isostatically pressed at 1650 °C for 3 h under 190 MPa argon gas pressure, and then the samples were annealed in air at 1350 °C for 10 h to compensate for oxygen vacancies. Both surfaces of the samples were mirror-polished for optical measurement. The samples were cut off using wire cutting perpendicular to the interface between undoped and doped regions, and mirror-polished on both sides for Nd ions concentration profile measurement across the interface.

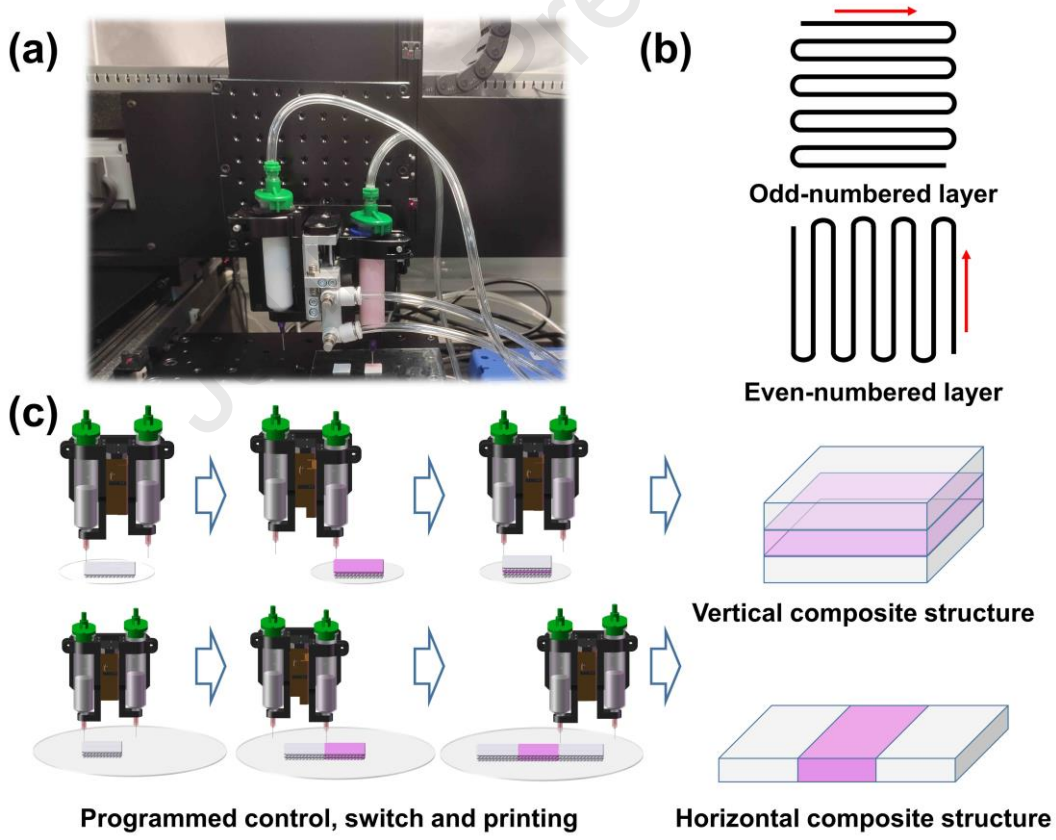

Fig. 2. (a) The photo of the homemade 3D printer, (b) printing path and (c) schematic diagram of the transparent composite ceramic green bodies prepared by direct ink

writing.

2.3. Characterization

The rheological properties of the slurries were characterized by a rotational rheometer (Haake Viscotester iQ Air, Thermo Electron GmbH, Germany) at 25 °C using a 20 mm diameter flat plate with the design gap of 0.1 mm. The printability of the slurry was evaluated by oscillation-rotation-oscillation (O.R.O.) test. The first stage was a low-shear oscillation test (Controlled Shear Deformation mode, frequency of 1 Hz, strain of 0.4%, 120 s). The second stage was a high-shear rotational test (Controlled Shear Rate mode, frequency of 1 Hz, shear rate of 85 s-1, 30 s). The third stage was identical to the first stage, lasting 300 s. The morphologies of the mixed powders, the fracture surfaces of the green bodies and the polished surfaces of the ceramics thermally etched at 1450 °C for 3 h were measured by scanning electron microscope (FEI Magellan 400, FEI, USA). The densities of the ceramics after vacuum pre-sintering were determined by the Archimedes principle method using water as the immersion liquid. The in-line transmittances of the double-face polished transparent ceramics were measured using a UV-VIS spectrometer (V-770, JASCO Corporation, Japan) over the wavelength range of 190 to 1100 nm. Due to the thin thickness of the horizontal composite sample, the in-line transmittances of the undoped and doped regions were measured separately. The average grain sizes of the composite ceramics in different regions were estimated by the linear intercept method based on the SEM images of polished and thermally etched ceramic surfaces. To ensure good measurement reliability, the grain size was estimated over at least 800 grains [27]. The Nd ions

concentration profiles across the interface of the transparent composite ceramics were measured by laser ablation-inductively coupled plasma-mass spectrometry (LA-ICP-MS), including a quadrupole-based X Series II ICP-MS system (Thermo Fisher, USA) and a NWR-213 laser ablation system (NewWave, USA). The laser experimental setup of the composite ceramics is shown in Fig. 3. The curvature of the collimating and focusing mirrors for the laser diode was 25 mm and 75 mm, respectively. The resonator consisted of an input mirror and a plane output coupler. The output couplers with the transmissions of 5.0% and 10.0% were used to measure laser performance. The transparent composite ceramics were cut into the dimension of 3×3 mm^2 in the cross-section area, and 4 mm in length. Furthermore, two end faces of the ceramics were carefully polished but uncoated. The ceramics were wrapped with the indium foil and mounted on a water-cooled copper heat sink maintained at a temperature of 20 °C to allow efficient heat removal. The samples were end pumped by a fiber-coupled laser diode with the emission wavelength around 808 nm.

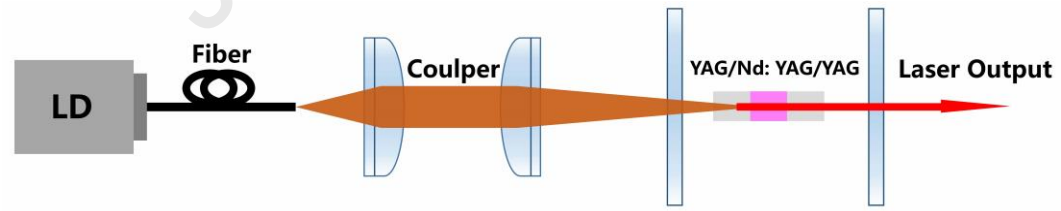

Fig. 3. Schematic diagram of the laser experimental setup.

3. Results and discussions

3.1. Slurries rheological behavior analysis

For ceramics by DIW, the increase of the solids loading of slurries can effectively reduce the possibility of deformation and cracking during the drying process of green

bodies. At the same time, the slurries should fill the void space between filaments and maintain the predefined profile in a proper range during printing. The fabrication details of the undoped YAG ceramic slurries were reported in Ref. [28], and results demonstrated that the overall performance of slurries with 50 vol. % solids loading was best. Therefore, to avoid excessive shrinkage stress between different components of green bodies during drying and sintering processes, the solids loading of the Nd: YAG ceramic slurry in this research was set to 50 vol. %.

The effect of dispersant content on the viscosity of Nd: YAG ceramic slurries was investigated as shown in Fig. 4(a). It can be observed that with the increase of the dispersant content, the viscosity of the slurries first decreases and then increases, and the optimum dispersant content is about 0.6 wt. % (relative to ceramic powder). This can be attributed to the fact that the electrostatic repulsion between ceramic particles increases with the increase of dispersant content. When the dispersant content is higher than the optimum content, the excess dispersant compresses the electric double layer, thereby reducing the electrostatic repulsion between particles. Also, the printability of the ceramic slurries with high solids loading and low viscosity can be effectively improved by adding HEC as a thickener, which is related to its content. The effect of HEC content on the static storage modulus and structural recovery capability of the Nd: YAG ceramic slurries was analyzed as shown in Figs. 4(b) and 4(c). G' and G" represent the storage modulus and loss modulus of the slurry, respectively. Based on authors' research results [28], ceramic slurries with the static storage modulus of more than 2300 Pa and good structural recovery capability were suitable for printing. As shown in Fig.

4(b), when the HEC content is 0.5 wt. % (relative to ceramic powder), the static storage modulus of the ceramic slurry reaches 2400 Pa. Moreover, in Fig. 4(c) the shear thinning behavior during the rotation stage can be observed in the oscillation-rotation-oscillation (O.R.O.) test, and the storage modulus can be quickly recovered after shearing. In conclusion, it was verified by rheological tests that the Nd: YAG ceramic slurry suitable for DIW was prepared by adding 0.5 wt. % HEC to the slurry with the high solids loading and low viscosity. Slurries with good printability were used to prepare composite ceramic green bodies, realizing the complete structures with clear outlines shown in Fig. 4(d).

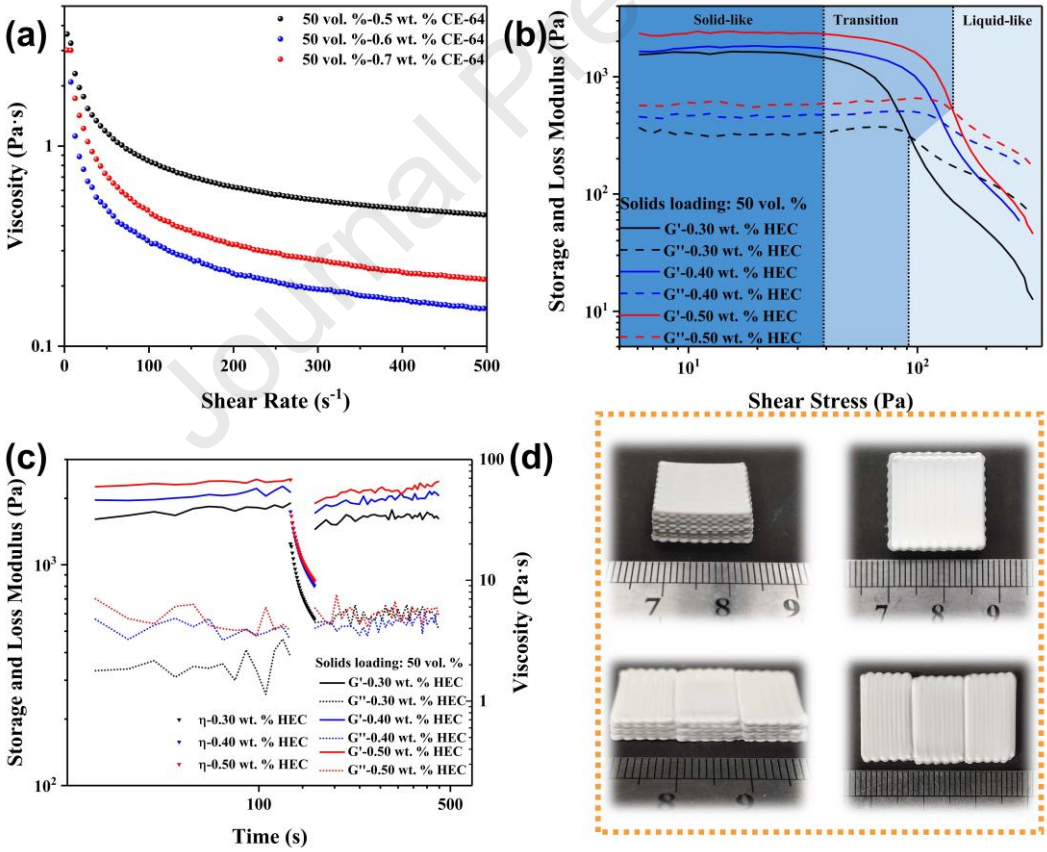

Fig. 4. (a) Effect of dispersant content on slurries viscosity, (b) amplitude sweep curves, and (c) O.R.O. curves of the slurries with different HEC addition, (d) photos

of vertical and horizontal composite ceramic green bodies.

3.2. Layer interface of green bodies

In the case of multilayer structural composites, the layer-by-layer fabrication often results in defective interfacial regions between different components, which deteriorates the performance. Tang *et al.* [29] found a clear interface in the cross section of the YAG/Yb: YAG/YAG composite ceramic green body, which was considered as the main scattering source in transparent ceramics. It was observed that there were numerous pores over the surfaces of the green tapes, and defects were easily formed at the interface during the stacking and laminating process. In this work, the samples were printed filament by filament so that the slurry exit from the nozzle worked as a continuous, rod-like filament with a rigid core-fluid shell architecture, allowing the filaments to fuse together at their contact points. This not only ensured the structural integrity of the composite material, but also reduced defects such as pores at the interface. Figs. 5(a) and (b) show the observed regions of vertical and horizontal composite ceramic green bodies near the interfaces between different components. Figs. 5(b-c) and (e-f) show the cross-section microstructures of the vertical and horizontal composite ceramic green bodies. It is noted that there are no obvious defects in the interface region between adjacent layers of different components. The close packing of particles in the green bodies is attributed to the low content of organic matter and high solids loading of the slurries, which is beneficial for the subsequent densification process.

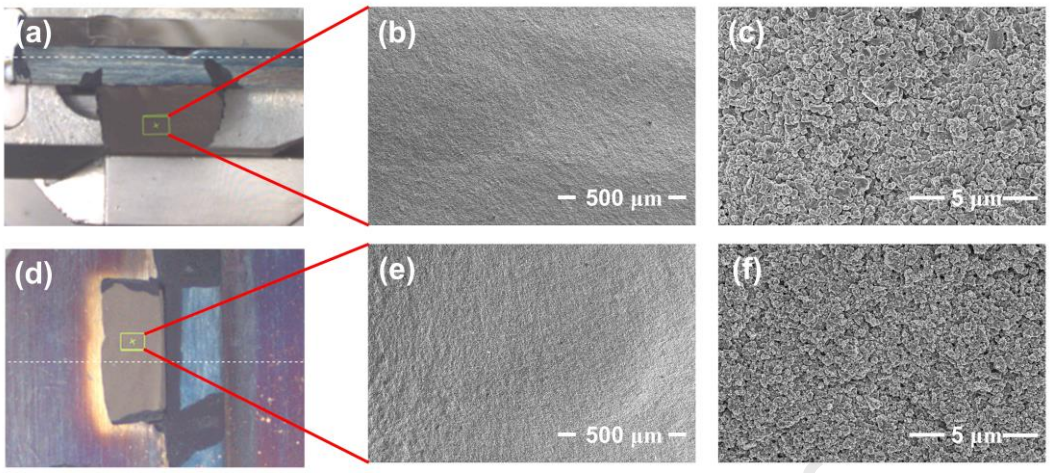

Fig. 5. Photographs of the (a) vertical composite and (b) horizontal composite green bodies on the sample table, SEM micrographs of the fracture surface of (b), (c) vertical composite and (c), (d) horizontal composite green bodies.

3.3. Sintering behaviors of single-component transparent ceramics

In order to fabricate the Nd: YAG transparent composite ceramics with high optical quality, the densification behavior of each layer with different composition has to be strictly controlled. Especially, when HIP is applied, the vacuum pre-sintering temperature needs to be carefully selected for ceramics with different doping concentrations. Therefore, the sintering densification processes of single-component transparent ceramics prepared from DIW were first investigated. In Fig. 6, it is observed that the relative densities of the Nd: YAG transparent ceramics at all different vacuum pre-sintering temperatures are higher than that of the undoped YAG transparent ceramics. For the Nd: YAG ceramics, Nd ions can replace Y ions in the lattice during sintering. As the radius of Nd ions (0.1109 nm) is larger than that of Y ions (0.1019 nm), such substitution could cause the lattice distortion of YAG to increase its system instability, leading to a decline of the sintering temperature of YAG [9]. Moreover,

Nd_2O_3 could form a liquid phase with SiO_2, which may increase the amount of liquid phase presence, leading to enhanced liquid phase sintering and increased densification [30, 31]. As a result, the sintering activity of the Nd: YAG ceramics is higher than that of undoped YAG ceramics. Under high temperature and pressure conditions, the intergranular pores can be effectively compressed and removed to improve the optical quality of transparent ceramics. Therefore, several pre-sintered samples with the apparent porosity close to 0 (the area selected by the oval box) were selected for the post-HIP treatment at 1650 °C.

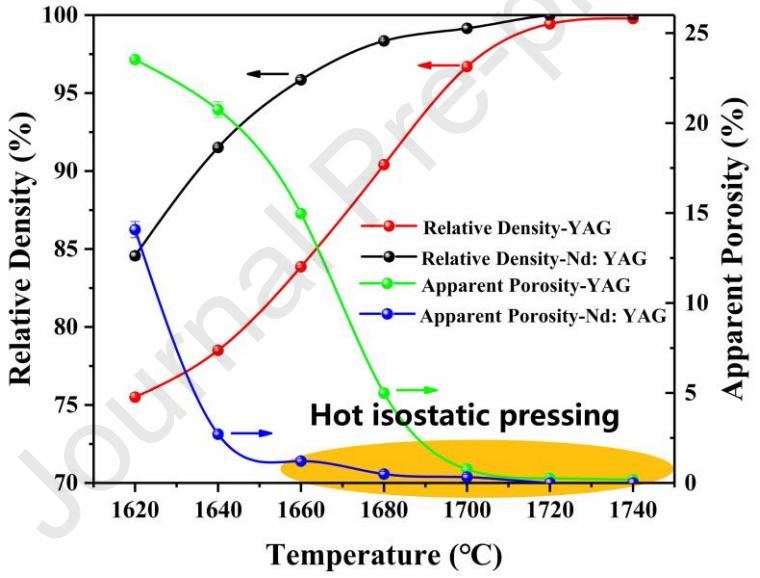

Fig. 6. Relative density and apparent porosity of the YAG and Nd: YAG ceramics at different vacuum pre-sintering temperatures for 6 h.

3.4. Optical properties of single-component and transparent composite ceramics

In order to obtain the high optical quality transparent composite ceramics, it is necessary to enhance the transparency of each component layer and ensure the overall quality of ceramics. The in-line transmittance curves of undoped YAG and Nd: YAG ceramics after hot isostatic pressing at 1650 °C for 3 h are shown in Figs. 7(a) and 7(b),

respectively. For the undoped YAG transparent ceramics, the in-line transmittances of the samples processed by vacuum pre-sintering at 1700 °C and 1720 °C shown in Fig. 7(a) are more than 80.6% at the visible wavelength of 400 nm, and further reach 83.2% at the wavelength shifting towards 1064 nm. The similar conclusion can also be drawn for the Nd: YAG transparent ceramics. The optical qualities of the samples obtained by vacuum pre-sintering at 1680 °C and 1700 °C are compared to explore the effect of pre-sintering temperature. In Fig. 7(b), the in-line transmittances of the transparent ceramic at 400 nm and 1064 nm are 82.7% and 84.2%, respectively. The strongest absorption peak at 808 nm well agrees with the characteristic absorption peak of Nd ions, which is ascribed to the electron transitions in the process of $^4I_{9/2} \rightarrow {}^2H_{9/2}+{}^4F_{5/2}$.

Compared with the Nd: YAG transparent ceramics, the in-line transmittances of the undoped YAG transparent ceramics are lower, so their optimal vacuum pre-sintering temperature may need further refinement. Moreover, it is expected that the high optical quality of transparent composite ceramics can be achieved by adjusting the types and compositions of sintering additives in different component ceramics. Summarily, considering the in-line transmittances of both undoped YAG and Nd: YAG transparent ceramics, the vacuum pre-sintering temperature was selected as 1700 °C to fabricate the transparent composite ceramics.

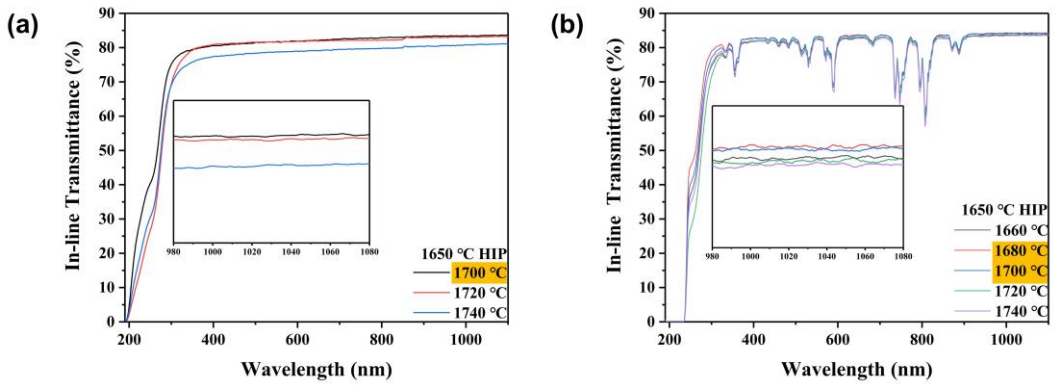

Fig. 7. In-line transmittance curves of the 3 mm thick polished (a) undoped YAG and (b) Nd: YAG transparent ceramics at different vacuum pre-sintering temperatures followed by 1650 °C HIP.

Figs. 8(a) and 8(b) provide the appearances and in-line transmittance curves of the transparent composite ceramics, respectively. It can be noted that the Nd: YAG regions of two composite ceramics present translucent after vacuum pre-sintering at 1700 °C, owing to the high relative density (>99%), while the undoped YAG regions shown in Fig. 8(a) do not demonstrate this behavior. In Fig. 8(b), the in-line transmittances of these two transparent composite ceramics reach more than 83.1% at 1064 nm. However, the absorption peak intensities around 808 nm are remarkably different. The absorption peak intensity of the horizontal transparent composite ceramic at 808 nm represents a higher value than that of vertical transparent composite ceramic. This can be explained by the larger thickness of the Nd: YAG region in the horizontal composite ceramic than that in the vertical composite ceramic.

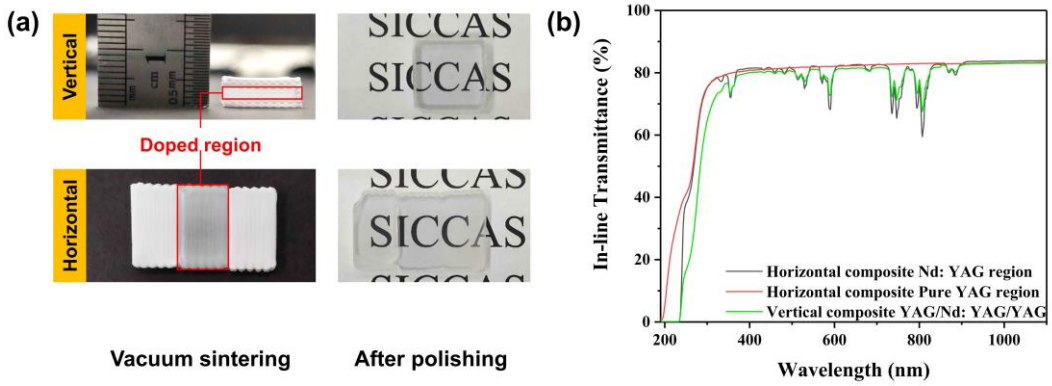

Fig. 8. (a) Appearances and (b) in-line transmittance curves of 4 mm thick vertical composite and 2 mm thick horizontal transparent composite ceramics.

3.5. Microstructures of transparent composite ceramics

In Fig. 9, the polished and thermally etched surfaces of the vertical and horizontal composite ceramics were obtained by SEM. For these two samples, the average grain sizes in the undoped YAG region were tested and calculated to be 2.03 μm and 2.45 μm, respectively. The average grain sizes in the Nd: YAG region increased to 4.13 μm and 3.59 μm, respectively, approximately 1.5 to 2 times larger than those in the undoped YAG region. The difference in the average grain size of the undoped YAG and Nd: YAG regions agrees with the change in the sintering behaviors of the single-component ceramics as the addition of Nd_2O_3 accelerates the sintering and densification processes and grain growth rates [31]. Moreover, it is found that there are no obvious pores or second phases present on the thermally etched surfaces.

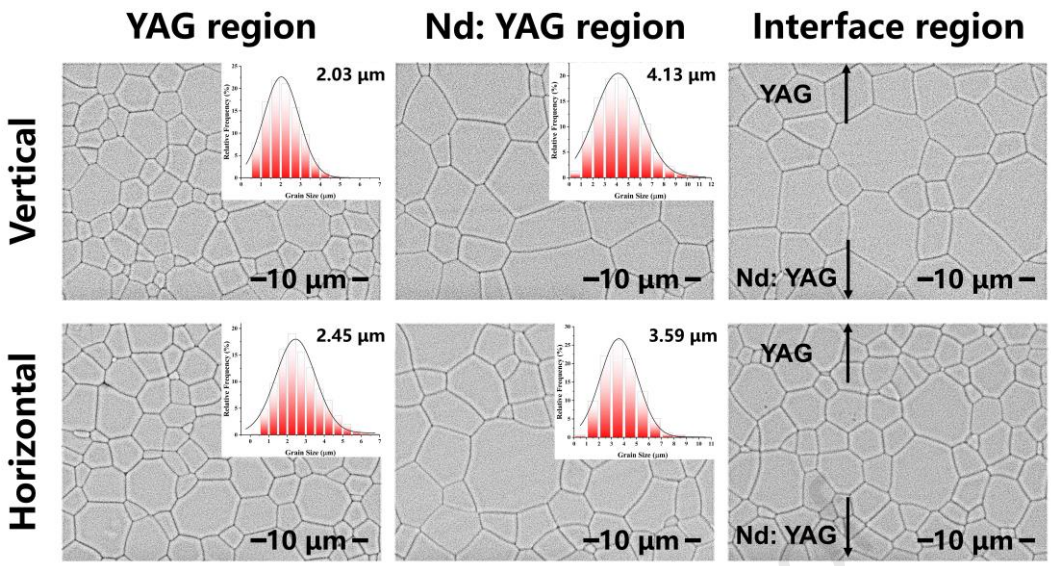

Fig. 9. SEM micrographs of the thermally etched surface of vertical and horizontal composite ceramics.

3.6. Diffusion behavior of Nd ions across the interface

Generally, the diffusion distance of ions depends on the sintering temperature and dwell time. For transparent composite ceramics, the diffusion of laser active ions between the interfaces of the undoped and doped regions needs to be strictly controlled. Investigations on the diffusion behavior are important for the understanding of optical properties of transparent composite ceramics, contributing to a clear guidance to the fabrication of gain medium for high-power solid laser. The diffusion process in polycrystalline materials can be classified into three types denoted as Harrison type A, B, and C. The transparent composite ceramics corresponds to type B [32]. For ceramics, it is a complicated process to be clearly understood, as there are two diffusion mechanisms, namely the volume diffusion and the grain boundary diffusion. The concentration profile can be described using Fick's one-dimensional diffusion equation. The transfer rate of diffusing ions through a unit area is proportional to the

concentration gradient [33], which can be calculated by Eq. (1):

$$\frac{\partial c}{\partial t} = D\frac{\partial^2 c}{\partial x^2} \tag{1}$$

where c (t, x) is the concentration, x denotes the space coordinate along the diffusion direction and D means the diffusion coefficient.

As the diffusion distance of ions is much smaller than the physical size of the transparent composite ceramics, the semi-infinite diffusion couple model shown in Fig. 10 can be used to analyze the concentration profile. The initial state is defined by Eq. (2) as follows:

$$c\,(t=0,x) = \begin{cases} c_0\,(\text{const}) & x \le x_0 \\ 0 & x \ge x_0 \end{cases} \tag{2}$$

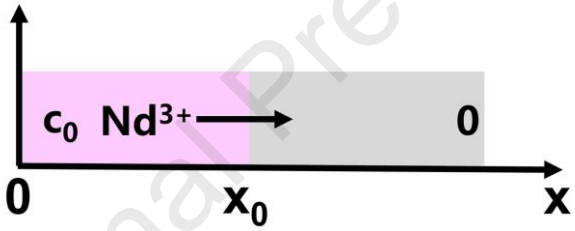

Fig. 10. Schematic diagram of the semi-infinite diffusion couple.

Also, the solution [33] to this diffusion problem is usually defined by Eqs. (3) and (4):

$$c(t, x) = \frac{c_0}{2}\left\{1 - \frac{2}{\sqrt{\pi}}\int_0^{\frac{x-x_0}{2\sqrt{Dt}}} \exp(-z^2)dz\right\} = \frac{c_0}{2}\operatorname{erfc}\left(\frac{x-x_0}{2\sqrt{Dt}}\right) \tag{3}$$

$$\alpha = \frac{1}{2\sqrt{Dt}} \tag{4}$$

where α is an intermediate variable.

Thus, the average diffusion distance $\langle x \rangle$ can be calculated by Eq. (5):

$$\langle x \rangle = \frac{1}{\alpha\sqrt{\pi}} \tag{5}$$

Usually, the average diffusion distance can be obtained by measuring the

concentration profile of Nd ions. However, due to the low doping concentration and the detection limit of Energy Dispersive Spectrometer, scanning electron microscopy cannot be used to characterize its concentration profile, but LA-ICP-MS has become an attractive analytical technique, owing to its direct analysis of solid samples, high sensitivity and low detection limits. Therefore, in the current work, LA-ICP-MS was used to characterize the concentration profile of Nd ions in the transparent composite ceramics. By measuring the spectrum intensity of the Nd element across the interface, the diffusion distance of Nd ions can be calculated using Eqs. (6) and (7):

$$I \propto c(t,x) \propto \operatorname{erfc}\left(\frac{x-x_0}{2\sqrt{Dt}}\right) \tag{6}$$

$$I(x) = I_0 \operatorname{erfc}\{\alpha(x-x_0)\} \tag{7}$$

The laser ablation inductively coupled plasma mass spectra of the transparent composite ceramics are provided in Fig. 11. As the horizontal composite ceramic was too long, only one side of the interface area was tested. It is noted that the experimental results well agree with the solid curves by Eq. (7).

In this research, Nd ions diffused to the undoped YAG region through the boundary of the Nd: YAG/YAG composite ceramics. The Nd ions diffusion distances of the vertical and horizontal composite ceramics were measured at the levels of 50.1 μm and 43.5 μm, respectively. Rudzik *et al.* [34] fabricated composite YAG/Nd: YAG ceramic by dry pressing and vacuum pre-sintering followed by HIP. In their work, the Nd ions diffusion distance obtained was about 40 μm. The shorter diffusion distance was due to the lower vacuum pre-sintering temperature under the same SiO_2 addition. Yagi *et al.* [35] polished two ceramics that were vacuum pre-sintered at 1400 °C and then diffusion

bonded at 1700 °C to get the YAG/Nd: YAG transparent composite ceramic. The diffusion distance of Nd ions from the contact interface was reported to be 17.7 μm, which was much shorter than that in this work. This could be interpreted by more SiO_2 addition, which led to the enhanced diffusivity of Nd ions for the generation of vacancy defects (i.e., V_Y''') and the segregation of Si ions at the grain boundaries [36]. Another possibility is the enhanced Nd diffusion during the sintering of the nanoparticles which make up the composite ceramic green body versus the diffusion bonding of already fully dense transparent ceramics with micron-scale grain sizes. In summary, DIW successfully achieves a controllable distribution of active ions around the interface between undoped and doped regions.

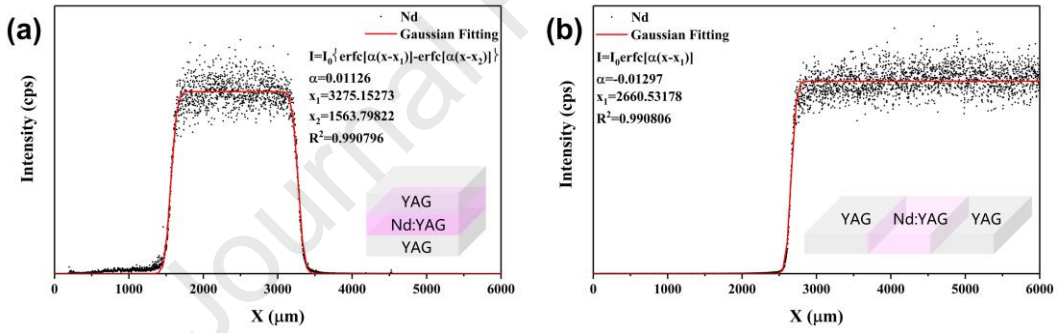

Fig. 11. Laser ablation inductively coupled plasma mass spectra of (a) vertical and (b) horizontal transparent composite ceramics.

3.7. Laser performances of transparent composite ceramics

Problems including the poor printability of slurries, any defects generated in the green bodies during the printing and the uncontrolled densification process of ceramics with different components, will limit the laser output power of composite laser ceramics. As laser performance is the key property of laser ceramics for their industrial applications, it is necessary to assess the effectiveness, feasibility and laser

performances of the fabricated ceramics. Fig. 12 demonstrates the remarkable relationship between the output power and the absorbed pump power of the vertical transparent composite ceramics with the output coupler transmission of 5.0% and 10.0%. For the transmission of 5.0%, the maximum output power of 1.67 W was obtained under the absorbed pump power of 5.68 W. The corresponding slope efficiency of 31.3% was also identified. The maximum output power of 2.15 W was achieved under the absorbed pump power of 5.70 W under the transmission of 10.0%. The corresponding slope efficiency increased to 40.2%. The limitation of laser slope efficiency can be attributed to the poor optical quality of the undoped YAG region, which can be seen from the in-line transmittance test results. Even so, the laser slope efficiency of the composite ceramic prepared in this research is far higher than the values reported by other 3D printed bulk composite laser ceramics, as listed in Table 1. Actually, the optical quality of transparent ceramics prepared from additive manufacturing techniques in most of the literature is not good enough to achieve effective laser output. Jones et al. first fabricated transparent composite ceramics using direct ink writing [21]. However, the slurry contained more than 50 vol. % organics, resulting in significant porosity in the green body after debinding, which could not be entirely eliminated through cold isostatic pressing. In addition, an excessively high pre-sintering temperature was employed, which is unreasonable. Based on our viewpoint, under high pre-sintering temperatures, pores were prone to becoming trapped in the grain, which cannot be eliminated by hot isostatic pressing sintering. Subsequently, Seeley et al. from the same team optimized the sintering protocol and the transparent

composite ceramic achieved laser output [17]. The primary reason affecting the laser performance of transparent composite ceramics was believed to be refractive index variations. Hostaša et al. used a slurry containing 58 vol. % organics, resulting in a green body with low density and a large number of pores [37]. To achieve full densification of the ceramic, an excessively high sintering temperature was employed, and the grain size exhibited abnormal growth, reaching 28.7 μm. Due to the defects in the green body and the inappropriate sintering protocol, the in-line transmittance of the polished ceramic was very low (<50%), indicating serious scattering losses, which affected the laser performance. In this study, a water-based slurry with high solids loading, low organic content (<1.6 wt. %) and excellent printability was utilized. The green body after debinding demonstrated high density and few defects. Furthermore, the sintering protocol was optimized by investigating the densification process of undoped YAG and Nd: YAG ceramics. These improvements collectively contributed to enhancing the laser performance of the composite ceramics.

Furthermore, future work on the reduced sintering densification difference between the ceramics with different components by adjusting the type or composition of sintering aids can be carried out. Theoretically, the laser efficiency of the transparent composite ceramic can be further enhanced by the optimal transmittance of the output coupler and the reduction of the cavity loss by antireflection-coating.

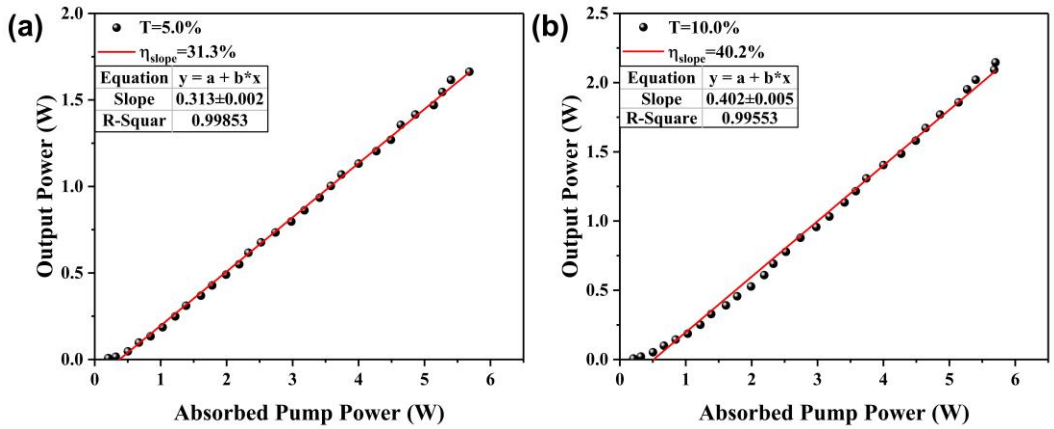

Fig. 12. Laser output power at 1064 nm as a function of the absorbed pump power for the vertical transparent composite ceramic with output coupler transmission of (a) 5.0% and (b) 10.0%.

Table 1 Comparison of laser ceramics prepared by additive manufacturing

Method	Slurry solids loading (vol. %)	Composition	Structure	Relative density (%)	Grain size (μm)	Slope efficiency (%)	Ref.
Direct ink writing	50	YAG/0.3 at. % Nd: YAG/YAG	Three-layered	100	3.0	40.2	This work
Direct ink writing	45	YAG/2.0 at. % Nd: YAG	Top-hat	-	-	~15.0	[17]
Direct ink writing	45	YAG/2.0 at. % Nd: YAG	Top-hat	100	-	-	[21]
Stereo-lithography	42	10 at. % Yb: YAG	Uniformly doped	-	28.7	17.6	[37]

4. Conclusion

YAG/0.3 at. % Nd: YAG/YAG transparent composite ceramics were successfully fabricated by a systematic investigation including the dual-material switching assisted DIW, vacuum sintering and hot isostatic pressing. The rheological experimental results showed that the optimal dispersant content was 0.6 wt. % and the ceramic slurries with good printability were obtained by adding 0.5 wt. % cellulose. It was noted that there were no observable defects in the interface region between the layers of different

components and the particles were fully close-packed in the green bodies. To further improve the optical quality of the transparent composite ceramics, the sintering behaviors of the undoped YAG and Nd: YAG ceramics were investigated to identify the optimal vacuum pre-sintering temperature of 1700 °C. Moreover, the composite ceramics by post hot isostatic pressing and annealing exhibited the in-line transmittance of more than 80.1% at 400 nm and up to 83.1% at 1064 nm. Finally, the Nd ions diffusion distances of the vertical and horizontal composite ceramics prepared from DIW were tested and calculated to be approximately 50.1 μm and 43.5 μm, respectively. With the absorbed pump power of 5.70 W, the maximum output power of 2.15 W at 1064 nm was generated with a slope efficiency of 40.2%. In conclusion, the proposed systematic investigation sheds light on an instructive approach to the fabrication of transparent composite ceramics, and also provides useful insight into the improvement of laser properties for wider applications of transparent composite ceramics.

Acknowledgements

This work was supported by National Key Research and Development Program of China (Grant No. 2023YFB3812000), National Natural Science Foundation of China (Grant No. 62405345), the Postdoctoral Fellowship Program of CPSF (Grant No. GZC20232830).

Declaration of competing interest

The authors have no competing interests to declare that are relevant to the content of this article.

References

[1] Y.S. Wu, J. Li, Y.B. Pan, J.K. Guo, B.X. Jiang, Y. Xu, J. Xu, Diode-pumped Yb: YAG ceramic laser, J. Am. Ceram. Soc. 90 (2007) 3334-3337, https://doi.org/10.1111/j.1551-2916.2007.01885.x.

[2] A.A. Kaminskii, Laser crystals and ceramics: recent advances, Laser & Photonics Reviews 1 (2007) 93-177, https://doi.org/10.1002/lpor.200710008..

[3] A. Ikesue, Y.L. Aung, Ceramic laser materials, Nature Photon. 2 (2008) 721-727, https://doi.org/10.1038/nphoton.2008.243.

[4] A. Ikesue, I. Furusato, K. Kamata, Fabrication of polycrystalline, transparent YAG ceramics by a solid-state reaction method, J. Am. Ceram. Soc. 78 (1995) 225-228, https://doi.org/10.1111/j.1151-2916.1995.tb08389.x.

[5] H.M. Yang, G.Y. Feng, S.H. Zhou, Thermal effects in high-power Nd: YAG disk-type solid state laser, Opt. Laser. Technol. 43 (2011) 1006-1015, https://doi.org/10.1016/j.optlastec.2011.01.005.

[6] I. Shoji, Y. Sato, S. Kurimura, V. Lupei, T. Taira, A. Ikesue, K. Yoshida, Thermal-birefringence-induced depolarization in Nd: YAG ceramics, Opt. Lett. 27 (2002) 234-236, https://doi.org/10.1364/OL.27.000234.

[7] W. Koechner, Thermal lensing in a Nd: YAG laser rod, Appl. Optics. 9 (1970) 2548-2553, https://doi.org/10.1364/AO.9.002548.

[8] F. Tang, Y.G. Cao, J.Q. Huang, H.G. Liu, W. Guo, W.C. Wang,

Fabrication and laser behavior of composite Yb: YAG ceramic, J. Am. Ceram. Soc. 95 (2012) 56-59, https://doi.org/10.1111/j.1551-2916.2011.04956.x.

[9] W.B. Liu, Y.P. Zeng, J. Li, Y. Shen, Y. Bo, N. Zong, P.Y. Wang, Y.D. Xu, J.L. Xu, D.F. Cui, Q.J. Peng, Z.Y. Xu, D. Zhang, Y.B. Pan, Sintering and laser behavior of composite YAG/Nd: YAG/YAG transparent ceramics, J. Alloy. Compd. 527 (2012) 66-70, https://doi.org/10.1016/j.jallcom.2012.02.161.

[10] B.Y. Ma, W. Zhang, B.Z. Shen, Y.Z. Wang, H.Z. Song, F. Li, X.M. Xie, Z.B. Zhang, Y.Q. Yang, Z.G. Guan, Preparation and characterization of highly transparent Nd: YAG/YAG composite ceramics, Opt. Mater. 79 (2018) 63-71, https://doi.org/10.1016/j.optmat.2018.03.023.

[11] J. Li, Y.S. Wu, Y.B. Pan, W.B. Liu, L.P. Huang, J.K. Guo, Laminar-structured YAG/Nd: YAG/YAG transparent ceramics for solid-state lasers, Int. J. Appl. Ceram. Tec. 5 (2008) 360-364, https://doi.org/10.1111/j.1744-7402.2008.02244.x.

[12] J. Hostaša, A. Piancastelli, G. Toci, M. Vannini, V. Biasini, Transparent layered YAG ceramics with structured Yb doping produced via tape casting, Opt. Mater. 65 (2017) 21-27, https://doi.org/10.1016/j.optmat.2016.09.057.

[13] M. Li, H. Hu, Q.S. Gao, J.T. Wang, J. Zhang, Y.C. Wu, T.J. Zhou, L. Xu, C. Tang, N. Zhao, P. Liu, A 7.08-kW YAG/Nd: YAG/YAG composite

ceramic slab laser with dual concentration doping, IEEE. Photonics. J. 9 (2017) 1504010, https://doi.org/ 10.1109/JPHOT.2017.2712765.

[14] E.R. Kupp, G.L. Messing, J.M. Anderson, V. Gopalan, J.Q. Dumm, C. Kraisinger, T.G. Nikolay, L.D. Merkle, M. Dubinskii, V.K. Simonaitis-Castillo, G.J. Quarles, Co-casting and optical characteristics of transparent segmented composite Er: YAG laser ceramics, J. Mater. Res. 25 (2010) 476-483, https://doi.org/10.1557/JMR.2010.0069.

[15] Z. Chen, X.H. Sun, Y.P. Shang, K.Z. Xiong, Z.K. Xu, R.S. Guo, S. Cai, C.M. Zheng, Dense ceramics with complex shape fabricated by 3D printing: A review, J. Adv. Ceram. 10 (2021) 195-218, https://doi.org/10.1007/s40145-020-0444-z.

[16] Z. Zhao, G.X. Zhou, Z.H. Yang, X.Q. Cao, D.C. Jia, Y. Zhou, Direct ink writing of continuous SiO2 fiber reinforced wave-transparent ceramics, J. Adv. Ceram. 9 (2020) 403-412, https://doi.org/10.1007/s40145-020-0380-y.

[17] Z. Seeley, T. Yee, N. Cherepy, A. Drobshoff, O. Herrera, R. Ryerson, S.A. Payne, 3D printed transparent ceramic YAG laser rods: Matching the core-clad refractive index, Opt. Mater. 107 (2020) 110121, https://doi.org/10.1016/j.optmat.2020.110121.

[18] G.R. Zhang, D. Carloni, Y.Q. Wu, 3D printing of transparent YAG ceramics using copolymer-assisted slurry, Ceram. Int. 46 (2020) 17130-17134, https://doi.org/10.1016/j.ceramint.2020.03.247.

[19] D. Carloni, G.R. Zhang, Y.Q. Wu, Transparent alumina ceramics fabricated by 3D printing and vacuum sintering, J. Eur. Ceram. Soc. 41 (2021) 781-791, https://doi.org/10.1016/j.jeurceramsoc.2020.07.051.

[20] H.H. Ji, H.T. Chen, B.H. Zhang, X.J. Mao, Y. Liu, J. Zhang, S.W. Wang, Direct ink writing of aluminium oxynitride (AlON) transparent ceramics from water-based slurries, Ceram. Int. 48 (2022) 8118-8124, https://doi.org/10.1016/j.ceramint.2021.12.014.

[21] I.K. Jones, Z.M. Seeley, N.J. Cherepy, E.B. Duoss, S.A. Payne, Direct ink write fabrication of transparent ceramic gain media, Opt. Mater. 75 (2018) 19-25, https://doi.org/10.1016/j.optmat.2017.10.005.

[22] J. Chen, H.H. Ji, J. Zhang, S.W. Wang, Y. Liu, Fabrication of YAG ceramic tube by UV-assisted direct ink writing, Ceram. Int. 48 (2022) 19703-19708, https://doi.org/10.1016/j.ceramint.2022.03.178.

[23] L.L. Lebel, B. Aissa, M.A.E. Khakani, D. Therriault, Ultraviolet-assisted direct-write fabrication of carbon nanotube/polymer nanocomposite microcoils, Adv. Mater. 22 (2010) 592-596, https://doi.org/10.1002/adma.200902192.

[24] L. Liu, Z. Xiong, Y.N. Yan, Y.Y. Hu, R.J. Zhang, S.G. Wang, Porous morphology, porosity, mechanical properties of poly(alpha-hydroxy acid)-tricalcium phosphate composite scaffolds fabricated by low-temperature deposition, J. Biomed. Mater. Res. Part A 82A (2007) 618-629, https://doi.org/10.1002/(sici)1097-4636(19990315)44:4<446::aid-

jbm11>3.0.co;2-f.

[25] A.M. Golobic, M.D. Durban, S.E. Fisher, M.D. Grapes, J.M. Ortega, C.M. Spadaccini, E.B. Duoss, A.E. Gash, K.T. Sullivan, Active mixing of reactive materials for 3D printing, Adv. Eng. Mater. 21 (2019) 1900147, https://doi.org/10.1002/adem.201900147.

[26] H.H. Ji, J. Zhao, J. Chen, S.Z. Shimai, H.T. Chen, G.H. Zhou, Y. Liu, J. Zhang, S.W. Wang, D.L. Yang, Direct ink writing of cellulose-plasticized aqueous ceramic slurry for YAG transparent ceramics, MRS. Commun. 12 (2022) 206-212, https://doi.org/10.1557/s43579-022-00163-y.

[27] Y.H. Dong, H.B. Yang, L. Zhang, X.Y. Li, D. Ding, X.H. Wang, J. Li, J.G. Li, I.W. Chen, Ultra-uniform nanocrystalline materials via two-step sintering, Adv. Funct. Mater. 31 (2021) 2007750, https://doi.org/10.1002/adfm.202007750.

[28] H.H. Ji, J. Zhao, J. Chen, S.Z. Shimai, J. Zhang, Y. Liu, D.Z. Liu, S.W. Wang, A novel experimental approach to quantitatively evaluate the printability of inks in 3D printing using two criteria, Addit. Manuf. 55 (2022) 102846, https://doi.org/10.1016/j.addma.2022.102846.

[29] F. Tang, Y.G. Cao, J.Q. Huang, W. Guo, H.G. Liu, Q.F. Huang, W.C. Wang, Multilayer YAG/Re: YAG/YAG laser ceramic prepared by tape casting and vacuum sintering method, J. Eur. Ceram. Soc. 32 (2012) 3995-4002, https://doi.org/10.1016/j.jeurceramsoc.2012.06.022.

[30] S.H. Lee, S. Kochawattana, G.L. Messing, J.Q. Dumm, G. Quarles, V.

Castillo, Solid-state reactive sintering of transparent polycrystalline Nd: YAG ceramics, J. Am. Ceram. Soc. 89 (2006) 1945-1950, https://doi.org/10.1111/j.1551-2916.2006.01051.x.

[31] S. Kochawattana, A. Stevenson, S.H. Lee, M. Ramirez, V. Gopalan, J. Dumm, V.K. Castillo, G.J. Quarles, G.L. Messing, Sintering and grain growth in SiO_2 doped Nd: YAG, J. Eur. Ceram. Soc. 28 (2008) 1527-1534, https://doi.org/10.1016/j.jeurceramsoc.2007.12.006.

[32] K. Fujioka, A. Sugiyama, Y. Fujimoto, J. Kawanaka, N. Miyanaga, Ion diffusion at the bonding interface of undoped YAG/Yb: YAG composite ceramics, Opt. Mater. 46 (2015) 542-547, https://doi.org/10.1016/j.optmat.2015.05.023.

[33] J. Crank, The Mathematics of Diffusion, 2nd ed. ed., Clarendon Press, Oxford (UK), 1975.

[34] T.J. Rudzik, Z.M. Seeley, F.J. Ryerson, N.J. Cherepy, S.A. Payne, Counter-ion effect on the diffusion behavior of Yb, Lu, and Nd ions in YAG transparent ceramics, Opt. Mater.:X. 13 (2022) 100132, https://doi.org/10.1016/j.omx.2021.100132.

[35] H. Yagi, K. Takaichi, K. Ueda, Y. Yamasaki, T. Yanagitani, A.A. Kaminskii, The physical properties of composite YAG ceramics, Laser. Phys. 15 (2005) 1338-1344.

[36] R. Boulesteix, A. Maitre, J.F. Baumard, Y. Rabinovitch, C. Salle, S. Weber, M. Kilo, The effect of silica doping on neodymium diffusion in

yttrium aluminum garnet ceramics: implications for sintering mechanisms, J. Eur. Ceram. Soc. 29 (2009) 2517-2526, https://doi.org/10.1016/j.jeurceramsoc.2009.03.003.

[37] J. Hostaša, M. Schwentenwein, G. Toci, L. Esposito, D. Brouczek, A. Piancastelli, A. Pirri, B. Patrizi, M. Vannini, V. Biasini, Transparent laser ceramics by stereolithography, Scr. Mater. 187 (2020) 194-196, https://doi.org/10.1016/j.scriptamat.2020.06.006.

Declaration of interests

☒ The authors declare that they have no known competing financial interests or personal relationships that could have appeared to influence the work reported in this paper.

☐ The author is an Editorial Board Member/Editor-in-Chief/Associate Editor/Guest Editor for *[Journal name]* and was not involved in the editorial review or the decision to publish this article.

☐ The authors declare the following financial interests/personal relationships which may be considered as potential competing interests: